

# LoRA-IR: Taming Low-Rank Experts for Efficient All-in-One Image Restoration

Yuang Ai<sup>♣,♡</sup> Huaibo Huang<sup>♣,♡†</sup> Ran He<sup>♣,♡</sup>

<sup>♣</sup>MAIS & NLPR, Institute of Automation, Chinese Academy of Sciences

<sup>♡</sup>School of Artificial Intelligence, University of Chinese Academy of Sciences

shallowdream555@gmail.com, huaibo.huang@cripac.ia.ac.cn, rhe@nlpr.ia.ac.cn

## Abstract

Prompt-based all-in-one image restoration (IR) frameworks have achieved remarkable performance by incorporating degradation-specific information into prompt modules. Nevertheless, handling the complex and diverse degradations encountered in real-world scenarios remains a significant challenge. To address this challenge, we propose LoRA-IR, a flexible framework that dynamically leverages compact low-rank experts to facilitate efficient all-in-one image restoration. Specifically, LoRA-IR consists of two training stages: degradation-guided pre-training and parameter-efficient fine-tuning. In the pre-training stage, we enhance the pre-trained CLIP model by introducing a simple mechanism that scales it to higher resolutions, allowing us to extract robust degradation representations that adaptively guide the IR network. In the fine-tuning stage, we refine the pre-trained IR network using low-rank adaptation (LoRA). Built upon a Mixture-of-Experts (MoE) architecture, LoRA-IR dynamically integrates multiple low-rank restoration experts through a degradation-guided router. This dynamic integration mechanism significantly enhances our model’s adaptability to diverse and unknown degradations in complex real-world scenarios. Extensive experiments demonstrate that LoRA-IR achieves state-of-the-art performance across 14 image restoration tasks and 29 benchmarks. Code and pre-trained models will be available at: <https://github.com/shallowdream204/LoRA-IR>.

## 1. Introduction

Image restoration (IR) is a fundamental task in computer vision, aiming to recover high-quality (HQ) images from degraded low-quality (LQ) inputs. In recent years, significant progress has been achieved with specialized restoration networks targeting specific degradations such as adverse weather removal [7, 15], denoising [83], deblurring

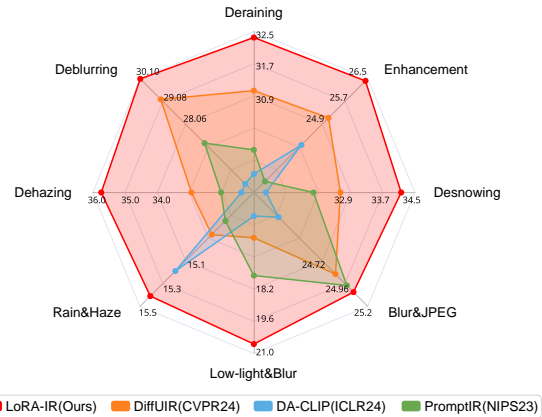


Figure 1. PSNR comparison with state-of-the-art all-in-one methods across 8 tasks (Tab. 4 and Tab. 9).

ring [58], and low-light enhancement [70]. However, in practical applications like autonomous driving and outdoor surveillance [40, 96], images are often simultaneously affected by multiple complex degradations, including haze, rain, snow, low-light conditions, and motion blur. These complex degradations not only degrade image quality but also severely impair the performance of downstream vision tasks, posing significant challenges to the safety and reliability of systems. Existing specialized models designed for single-task restoration struggle to generalize effectively in such unpredictable and variable environments.

To overcome the limitations of specialized models, there is increasing interest in developing all-in-one frameworks capable of handling diverse degradations. Early approaches, such as multi-encoder architectures [24] (Fig. 2 (a)), employ separate encoders for different degradation types. While effective in handling multiple degradations, their redundant structures lead to a large number of parameters, hindering scalability and efficiency. More recent methods adopt prompt-based frameworks [2, 33, 36, 48] (Fig. 2 (b)), encoding degradation-specific information into lightweight prompts to guide a shared network. However, relying solely on lightweight prompts and a static shared network may not fully capture the fine-grained de-

<sup>†</sup>Corresponding author.

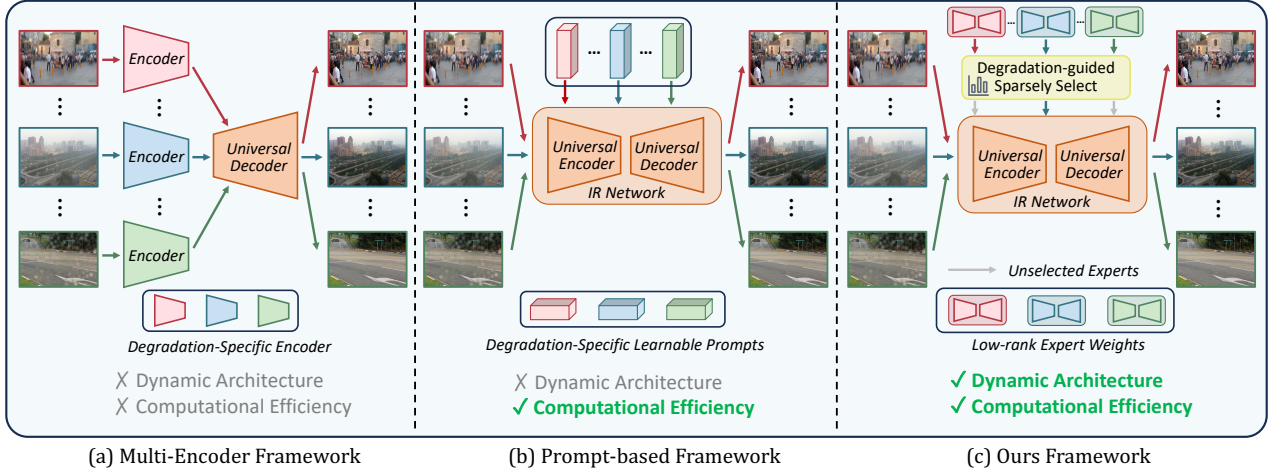


Figure 2. Conceptual comparison of all-in-one frameworks. (a) Multi-Encoder Structures: Use multiple encoders to extract features, but redundancy reduces computational efficiency. (b) Prompt-Based Methods: Employ lightweight prompts for degradation-specific features, improving efficiency. However, static network structures limit their ability to handle unknown complex degradations. (c) Our Proposed Framework: Dynamically and sparsely combines low-rank restoration experts. This design maintains computational efficiency while adapting flexibly to diverse degradation types, enhancing real-world performance.

tails and specific patterns associated with different degradations, leading to suboptimal restoration results. Furthermore, potential correlations and shared features among different degradations—such as common patterns in adverse weather conditions [80, 95]—are not extensively leveraged. Exploring these correlations could be key to enhancing model adaptability and effectiveness in complex real-world scenarios.

In this work, we propose LoRA-IR, a flexible framework for efficient all-in-one image restoration (Fig. 2 (c)). Motivated by the success of Low-Rank Adaptation (LoRA) [14] in parameter-efficient fine-tuning, this paper explores the use of diverse low-rank experts to model degradation characteristics and correlations efficiently. LoRA-IR consists of two stages of training, both guided by a proposed degradation-guided router (DG-Router). DG-Router is based on the powerful vision-language model CLIP [51], which has demonstrated strong representational capabilities across a wide range of high-level vision tasks [29, 90]. However, when applied to low-level tasks, its limited input resolution inevitably leads to suboptimal performance when handling high-resolution LQ images. To this end, we introduce a simple yet effective method for scaling CLIP to high resolution. Our approach involves downsampling the image and applying a sliding window technique to capture both global and local detail representations, which are subsequently fused using lightweight MLPs. With minimal training parameters and a short training time, DG-Router provides robust degradation representations and probabilistic guidance for the training of LoRA-IR.

In the first stage, we use the degradation representations provided by the DG-Router to guide the pre-training of

the IR network. The degradation representations dynamically modulate features within the IR network through the proposed degradation-guided adaptive modulator (DAM). In the second stage, we fine-tune the IR network obtained from the first stage using LoRA. Based on the Mixture-of-Expert (MoE) [53] structure, we construct a set of low-rank restoration experts. Leveraging the probabilistic guidance of the DG-Router, we sparsely select different LoRA experts to dynamically adjust the IR network. Different experts enhance the network’s ability to capture degradation-specific knowledge, while their collaboration equips the network with the capability to learn correlations between various degradations. The dynamic network structure enables LoRA-IR to adapt to diverse degradations and improves its generalization capabilities. As shown in Fig. 1, LoRA-IR outperforms all compared state-of-the-art all-in-one methods and demonstrates favorable generalizability in handling complex real-world scenarios.

The main contributions can be summarized as follows:

- We propose LoRA-IR, a simple yet powerful baseline for all-in-one restoration. LoRA-IR employs a novel mixture of low-rank expert structures, boosting architectural flexibility while maintaining computational efficiency.
- We propose a CLIP-based degradation-guided router (DG-Router) to extract robust degradation representations. DG-Router requires minimal training parameters and time, offering valuable guidance for LoRA-IR.
- Extensive experiments across 14 image restoration tasks and 29 benchmarks validate the SOTA performance of LoRA-IR. Notably, LoRA-IR exhibits strong generalizability to real-world scenarios, including training-unseen tasks and mixed-degradation removal.

## 2. Related Work

### 2.1. Image Restoration

Image restoration for known degradations has been extensively studied [4, 9, 26, 27, 65, 71, 77, 78, 82]. Recently, there has been significant interest in all-in-one frameworks within the community [60, 81, 95]. AirNet [22] is the pioneering work in all-in-one IR, utilizing contrastive learning to capture degradation information. Recent SOTA methods are mostly based on prompt learning, using lightweight prompts to encode degradation information. PromptIR [48] proposes a plug-and-play prompt module to guide the restoration process. DA-CLIP [36] utilizes a prompt learning module to incorporate degradation embeddings. MPerceiver [2] introduces a multi-modal prompt learning approach to harness Stable Diffusion priors. Despite achieving promising results, most existing methods use fixed network architectures, which may limit their ability to cover complex real-world scenarios.

### 2.2. Vision-Language Models

Vision-language models (VLMs) have demonstrated strong performance across various multi-modal and vision-only tasks [8, 29, 51]. Among them, CLIP, as a powerful VLM, has demonstrated impressive zero-shot and few-shot capabilities across various high-level vision tasks [66, 67, 93]. However, in low-level vision tasks, CLIP’s capabilities have been relatively less explored. DA-CLIP [36] is the first to introduce CLIP into all-in-one IR. It adopts a ControlNet-style [86] structure, using contrastive learning with image-text pairs to fine-tune CLIP. In this work, we focus on exploring CLIP’s visual representation capabilities to achieve efficient degradation representation. Compared to DA-CLIP (Tab. 7), our proposed DG-Router requires  $64\times$  fewer learning parameters and  $4\times$  less training time, while achieving superior performance.

### 2.3. Parameter-efficient Fine-tuning

With the rise of large foundational models [1, 18, 51] in modern deep learning, the community has increasingly shifted its focus towards parameter-efficient fine-tuning (PEFT) methods for effective model adaptation. Among these, prompt learning [20, 90] and Low-Rank Adaptation (LoRA) [14] are two prominent and widely used PEFT methods. As discussed above, prompt learning has been widely applied in low-level vision tasks. LoRA posits that the weight changes during model adaptation follow a low-rank structure and incorporates trainable rank decomposition matrices into the pre-trained model. Specifically, the change matrix is re-parameterized into the product of two low-rank matrices:  $W = W_0 + \Delta W = W_0 + sBA$ , where  $W_0$  represents pre-trained weight matrix,  $B \in \mathbb{R}^{m \times r}$  and  $A \in \mathbb{R}^{r \times n}$  are low-rank matrices,  $s = \frac{\alpha}{r}$  is the scaling fac-



Figure 3. Visualization of images output by the CLIP processor (top row from GoPro [44] and bottom row from LIVE1 [54]), which reveals significant loss of degradation information after processing. Please zoom in for a better view.

tor. In this work, we first introduce LoRA into the all-in-one frameworks to facilitate efficient image restoration.

## 3. Method

As shown in Fig. 4, the image restoration network is based on the commonly used U-Net [4, 65, 78] structure, consisting of stacked encoder, middle, and decoder blocks. Our LoRA-IR consists of two training stages: degradation-guided pre-training and parameter-efficient fine-tuning, both directed by the proposed degradation-guided router (DG-Router). We first introduce the CLIP-based DG-Router in Sec. 3.1, which is used to extract robust degradation representations and provide probabilistic estimates to guide the training of LoRA-IR. Then we detail the pre-training process of LoRA-IR in Sec. 3.2. Finally, we describe the fine-tuning process in Sec. 3.3.

### 3.1. Degradation-guided Router

As shown in Fig. 4 (a), DG-Router uses a pre-trained CLIP image encoder to extract rich features from LQ images. The pre-trained CLIP image encoder typically limits input images to a smaller resolution (e.g.,  $224 \times 224$ ). When handling higher-resolution images, a common approach [36] is to downsample the image to the resolution supported by CLIP using the processor. While this may have minimal impact on perception-based high-level classification tasks, significant downsampling can potentially lead to the loss of critical degradation information in pixel-level regression tasks like image restoration. Fig. 3 illustrates the results after the CLIP processor has processed the LQ images. It can be seen that significant downsampling leads to a substantial loss of degradation information in the LQ images, making it challenging to effectively extract degradation representa-

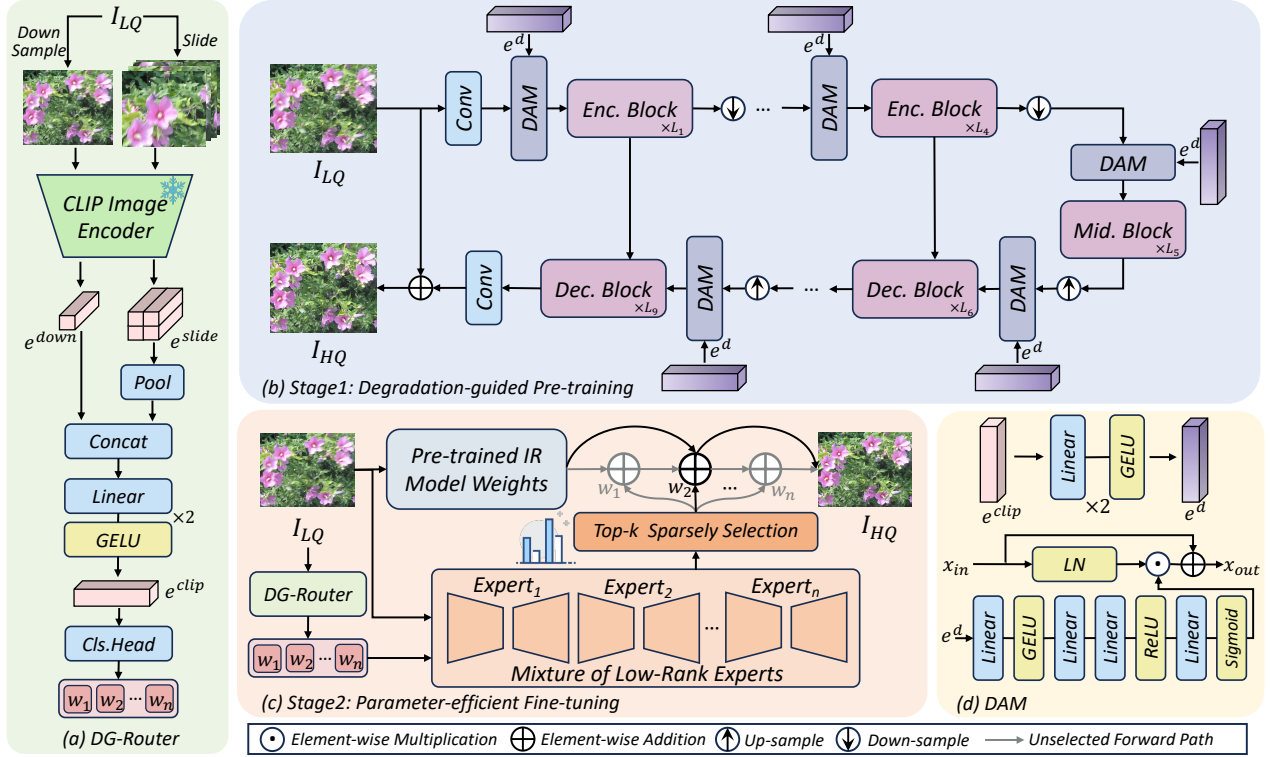


Figure 4. Overall of the proposed LoRA-IR, which includes (a) Degradation-guided router (DG-Router), (b) Pre-training image restoration network with robust degradation embedding, (c) Fine-tuning image restoration network with low-rank restoration experts, and (d) Degradation-guided adaptive modulator (DAM).

tokens from the CLIP output features.

To address this issue, we propose a simple yet effective mechanism for scaling up the input resolution. For input LQ image  $I_{LQ} \in \mathbb{R}^{H \times W \times 3}$ , we use a sliding window to partition the image into small local patches  $I_{slide} \in \mathbb{R}^{M \times H_c \times W_c \times 3}$ , where  $M$  is the number of patches,  $H_c \times W_c$  is the CLIP supported resolution. Both  $I_{slide}$  and down-sampled image  $I_{down} \in \mathbb{R}^{H_c \times W_c \times 3}$  are fed into the image encoder simultaneously, obtaining output features  $e^{slide} \in \mathbb{R}^{M \times C_{clip}}$  and  $e^{down} \in \mathbb{R}^{C_{clip}}$ . As depicted in Fig. 4 (a), after pooling  $e^{slide}$ , we concatenate them and pass them into a two-layer MLP to obtain the CLIP extracted degradation embedding  $e^{clip}$ , which can be formulated as

$$\begin{aligned} [e^{down}, e^{slide}] &= \text{CLIP}([I_{down}, I_{slide}]), \\ e^{clip} &= \text{MLP}(\text{Concat}(e^{down}, \text{Pooling}(e^{slide}))). \end{aligned} \quad (1)$$

After feeding  $e^{clip}$  into the classification head, we ultimately obtain the degradation prediction probability  $w \in \mathbb{R}^n$ , where  $n$  is the number of degradation types. Without bells and whistles, the DG-Router is optimized using standard cross-entropy loss, with the only parameters being the classification head and the two-layer MLP. Once training is complete, all parameters of the DG-Router are frozen and no longer updated.

### 3.2. Degradation-guided Pre-training

In the pre-training stage (Fig. 4 (b)), We dynamically modulate the restoration network using the degradation representations  $e^{clip}$  extracted by the DG-Router. We propose a degradation-guided adaptive modulator (DAM) to modulate the features of the restoration network. As shown in Fig. 4 (d), we first use a two-layer MLP projector to transform  $e^{clip}$  into a degradation embedding  $e^d$  in the feature space of the IR network. DAM adopts a structure similar to the channel attention block [88], modulating degradation information along the channel dimension, which can be formulated as

$$\begin{aligned} e^d &= \text{MLP}_{\text{shared}}(e^{clip}), \\ x_{out} &= \text{LN}(x_{in}) \odot \text{Sigmoid}(\text{MLP}(e^d)) + x_{in}, \end{aligned} \quad (2)$$

where  $\odot$  denotes the element-wise multiplication,  $\text{MLP}_{\text{shared}}$  denotes the MLP projector shared across different blocks, LN denotes LayerNorm,  $x_{in}$  is the original feature in the IR network, and  $x_{out}$  is the feature after modulation. Through the modulation of DAM, the robust degradation representations from the DG-Router can effectively enhance the degradation-specific knowledge of the IR network during pre-training.

### 3.3. Parameter-efficient Fine-tuning

In the fine-tuning stage, we aim to utilize the Low-Rank Adaptation (LoRA) technique to model degradation characteristics and correlations efficiently, enhancing the model’s ability to handle training-seen degradations and improving its robustness for real-world training-unseen degradations.

As shown in Fig. 4 (c), built upon the Mixture-of-Expert (MoE) architecture, we establish a collection composed of low-rank restoration experts. We have a total of  $n$  low-rank experts  $\{E_1, E_2, \dots, E_n\}$ , each expert is a learnable lightweight LoRA weight of the pre-trained restoration network from the first stage, specialized in handling a specific type of degradation.

For a given input LQ image, DG-Router can predict its degradation probability  $w \in \mathbb{R}^n$ .  $w$  is used as the score of different experts to select the appropriate expert for the restoration process. We sparsely select the top- $k$  highest-scoring experts as the most relevant ones and achieve the final restoration result through their dynamic collaboration, which can be formulated as

$$x_{out} = PreMod(x_{in}) + \sum_{i=1}^k w'_{\varphi(i)} E_{\varphi(i)}(x_{in}), \quad (3)$$

where  $PreMod$  denotes the pre-trained module in stage1,  $\varphi(i)$  denotes the index of the  $i$ -th selected expert,  $w' \in \mathbb{R}^n$  represents the result of reapplying softmax normalization to the scores of the selected top- $k$  experts (the weights of the experts that were not selected are set to 0).

Note that the sparse selection mechanism in Eq. (3) grants LoRA-IR a flexible network structure, enhancing its ability to represent degradation-specific knowledge. The dynamic combination mechanism, on the other hand, facilitates collaboration among different restoration experts, effectively modeling the commonalities and correlations between various degradations. The design of the low-rank experts ensures the efficiency of LoRA-IR, enabling it to achieve high-performance all-in-one image restoration in a computationally efficient manner.

## 4. Experiments

### 4.1. Experimental Setup

**Settings.** To comprehensively evaluate our method, we conduct experiments in five different settings following previous works: **(I) 4-task adverse weather removal** [56], including desnowing, deraining, dehazing, and raindrop removal; **(II) 3-task real-world adverse weather removal** [73], including deraining, dehazing, and desnowing; **(III) 3-task image restoration** [22], including deraining, dehazing, and denoising; **(IV) 5-task image restoration** [89], including deraining, low-light enhancement, desnowing, dehazing, and deblurring; **(V) 10-task image**

**restoration** [36], including deblurring, dehazing, JPEG artifact removal, low-light enhancement, denoising, raindrop removal, deraining, shadow removal, desnowing, and inpainting. For each setting, we train a unified model to handle multiple types of degradations.

**Datasets and Metrics.** For Setting I, we use the All-Weather [56, 60] dataset to evaluate our method. For Setting II, we use the WeatherStream [80] dataset to evaluate the model’s performance in real-world scenarios. For Setting III, we use RESIDE [21] for dehazing, WED [39] and BSD [41] for denoising, Rain100L [74] for deraining. For Setting IV, we use a merged dataset [78, 89] for deraining, LOL [68], DCIE [19], MEF [38], and NPE [62] for low-light enhancement, Snow100K [34] for desnowing, RESIDE [21] for dehazing, GoPro [44], HIDE [55], Real-Blur [52] for deblurring. For Setting V, we use the same dataset as [36]. We provide a detailed introduction to the datasets used for training and testing in Appendix.

As for evaluation metrics, we adopt PSNR and SSIM as the distortion metrics, LPIPS [87] and FID [13] as perceptual metrics. For benchmarks that do not include ground truth images, we use NIQE [42], LOE [61] and IL-NIQE [85] as no-reference metrics.

**Implementation Details.** For the training of DG-Router, we use the Adam optimizer with a batch-size of  $64 \times n$ , where  $n$  is the number of tasks. The whole training takes 20 minutes with a fixed learning rate of  $2e^{-4}$  using 8 NVIDIA A100 GPUs. Our LoRA-IR follows a two-stage training process, namely pre-training and fine-tuning. For both stages, we use the AdamW optimizer with a batch-size of 64. Following [36, 89], the training patch size is set to 256 to ensure fair comparisons. Random cropping, flipping, and rotation are used as data augmentation techniques. For the image restoration network structure, all basic blocks in Fig. 4 are the simple convolutional NAFBlocks [4], forming a simple all-in-one CNN baseline. More specific details for different settings provided in Appendix.

### 4.2. Comparison with State-of-the-Art Methods

**Setting I.** Tab. 1 shows the comparison results of our method with task-specific methods and all-in-one methods. Compared to SOTA methods like MPerceiver [2] and Histoformer [56], our approach shows significant improvements across all benchmarks and metrics. Visual comparisons are provided in the Appendix.

**Setting II.** To further demonstrate the effectiveness of our method in mitigating real-world adverse weather conditions, we evaluate its performance on the WeatherStream [80] dataset. Tab. 3 presents the quantitative comparison results of PSNR with SOTA general IR as well as all-in-one IR methods. Compared to the SOTA method LDR [73], our method achieves an average PSNR improvement of 0.76 dB across the three tasks. Visual comparisons

Table 1. [Setting I] Quantitative comparisons for *4-task adverse weather removal*. The top halves of the tables show task-specific results, while the bottom halves present all-in-one evaluations. LoRA-IR surpasses recent SOTA all-in-one techniques, including MPerceiver [2] and Histoformer [56], across all evaluated datasets and metrics.

(a) Image Desnowing					(b) Deraining & Dehazing			(c) Raindrop Removal		
	Snow100K-S [34]		Snow100K-L [34]			Outdoor-Rain [23]			RainDrop [49]	
	PSNR	SSIM	PSNR	SSIM		PSNR	SSIM		PSNR	SSIM
SPANet [63]	29.92	0.8260	23.70	0.7930	CycleGAN [94]	17.62	0.6560	pix2pix [16]	28.02	0.8547
JSTASR [5]	31.40	0.9012	25.32	0.8076	pix2pix [16]	19.09	0.7100	DuRN [32]	31.24	0.9259
RESCAN [25]	31.51	0.9032	26.08	0.8108	HRGAN [23]	21.56	0.8550	RaindropAttn [50]	31.44	0.9263
DesnowNet [34]	32.33	0.9500	27.17	0.8983	PCNet [17]	26.19	0.9015	AttentiveGAN [49]	31.59	0.9170
DDMSNet [84]	34.34	0.9445	28.85	0.8772	MPRNet[77]	28.03	0.9192	IDT [72]	31.87	0.9313
NAFNet [4]	34.79	0.9497	30.06	0.9017	NAFNet [4]	29.59	0.9027	MAXIM [59]	31.87	0.9352
Restormer [78]	36.01	0.9579	30.36	0.9068	Restormer [78]	30.03	0.9215	Restormer [78]	32.18	0.9408
All-in-One [24]	-	-	28.33	0.8820	All-in-One [24]	24.71	0.8980	All-in-One [24]	31.12	0.9268
TransWeather [60]	32.51	0.9341	29.31	0.8879	TransWeather [60]	28.83	0.9000	TransWeather [60]	30.17	0.9157
Chen <i>et al.</i> [6]	34.42	0.9469	30.22	0.9071	[6]	29.27	0.9147	[6]	31.81	0.9309
WGWSNet [95]	34.31	0.9460	30.16	0.9007	WGWSNet [95]	29.32	0.9207	WGWSNet [95]	32.38	0.9378
WeatherDiff <sub>64</sub> [46]	35.83	0.9566	30.09	0.9041	WeatherDiff <sub>64</sub> [46]	29.64	0.9312	WeatherDiff <sub>64</sub> [46]	30.71	0.9312
WeatherDiff <sub>128</sub> [46]	35.02	0.9516	29.58	0.8941	WeatherDiff <sub>128</sub> [46]	29.72	0.9216	WeatherDiff <sub>128</sub> [46]	29.66	0.9225
AWRCP [75]	36.92	0.9652	31.92	<b>0.9341</b>	AWRCP [75]	31.39	0.9329	AWRCP [75]	31.93	0.9314
MPerceiver [2]	36.23	0.9571	31.02	0.9164	MPerceiver [2]	31.25	0.9246	MPerceiver [2]	<u>33.21</u>	0.9294
Histoformer [56]	<u>37.41</u>	<u>0.9656</u>	<u>32.16</u>	0.9261	Histoformer [56]	<u>32.08</u>	<u>0.9389</u>	Histoformer [56]	<u>33.06</u>	<u>0.9441</u>
LoRA-IR (Ours)	<b>37.89</b>	<b>0.9683</b>	<b>32.28</b>	<u>0.9296</u>	LoRA-IR (Ours)	<b>32.62</b>	<b>0.9447</b>	LoRA-IR (Ours)	<b>33.39</b>	<b>0.9489</b>

Table 2. [Setting III] Quantitative comparison with all-in-one models for *3-task image restoration*.

Method	Dehazing on SOTS	Deraining on Rain100L	Denosing on BSD68 dataset			Average
			$\sigma = 15$	$\sigma = 25$	$\sigma = 50$	
BRDNet [57]	23.23 / 0.895	27.42 / 0.895	32.26 / 0.898	29.76 / 0.836	26.34 / 0.836	27.80 / 0.843
LPNet [12]	20.84 / 0.828	24.88 / 0.784	26.47 / 0.778	24.77 / 0.748	21.26 / 0.552	23.64 / 0.738
FDGAN [10]	24.71 / 0.924	29.89 / 0.933	30.25 / 0.910	28.81 / 0.868	26.43 / 0.776	28.02 / 0.883
MPRNet [77]	25.28 / 0.954	33.57 / 0.954	33.54 / 0.927	30.89 / 0.880	27.56 / 0.779	30.17 / 0.899
DL [11]	26.92 / 0.391	32.62 / 0.931	33.05 / 0.914	30.41 / 0.861	26.90 / 0.740	29.98 / 0.875
AirNet [22]	27.94 / 0.962	34.90 / 0.967	33.92 / 0.933	31.26 / 0.888	28.00 / 0.797	31.20 / 0.910
PromptIR [48]	30.58 / <b>0.974</b>	36.37 / 0.972	33.98 / 0.933	31.31 / 0.888	28.06 / 0.799	32.06 / 0.913
LoRA-IR (Ours)	<b>30.68</b> / 0.961	<b>37.75</b> / <b>0.979</b>	<b>34.06</b> / <b>0.935</b>	<b>31.42</b> / <b>0.891</b>	<b>28.18</b> / <b>0.803</b>	<b>32.42</b> / <b>0.914</b>

Table 3. [Setting II] Quantitative comparisons for *3-task real-world adverse weather removal* on WeatherStream [80].

Method	Rain	Haze	Snow	Average
MPRNet [77]	21.50	21.73	20.74	21.32
NAFNet [4]	23.01	22.20	22.11	22.44
Uformer [65]	22.25	18.81	20.94	20.67
Restormer [78]	23.67	22.90	22.51	22.86
GRL [26]	23.75	22.88	22.59	23.07
AirNet [22]	22.52	21.56	21.44	21.84
TUM [6]	23.22	22.38	22.25	22.62
Transweather [60]	22.21	22.55	21.79	22.18
WGWS [95]	23.80	22.78	22.72	23.10
LDR [73]	<u>24.42</u>	<u>23.11</u>	<u>23.12</u>	<u>23.55</u>
LoRA-IR (Ours)	<b>25.22</b>	<b>24.39</b>	<b>23.31</b>	<b>24.31</b>

are provided in the Appendix.

**Setting III.** Tab. 2 presents the quantitative comparison results for 3-task image restoration. Our method surpasses PromptIR [48] by 1.38 dB in PSNR and 0.007 in SSIM on the Rain100L dataset, with an average improvement of 0.36

dB across the three tasks. Visual comparisons are provided in the Appendix.

**Setting IV.** Tab. 4 presents the quantitative comparison results of our method against SOTA task-specific methods and all-in-one methods across five tasks. It shows that our method outperforms the compared all-in-one methods across all tasks and even surpasses task-specific methods in the majority of tasks. For example, compared to the recent SOTA method DiffUIR [89], LoRA-IR brings a PSNR improvement ranging from 0.92 to 2.8 dB across various tasks.

To further validate the generalizability of our method for complex degradations in real-world scenarios, we evaluate from two perspectives:

(1) **Generalization on Training-seen Tasks:** We directly test the trained all-in-one model on real-world benchmarks that were not seen during training. As shown in Tab. 5, our method achieves the best PSNR and SSIM metrics in deblurring tasks. As discussed in [69, 76], diffusion-based IR methods typically have an advantage in no-reference metrics like NIQE. However, our CNN-based model achieves

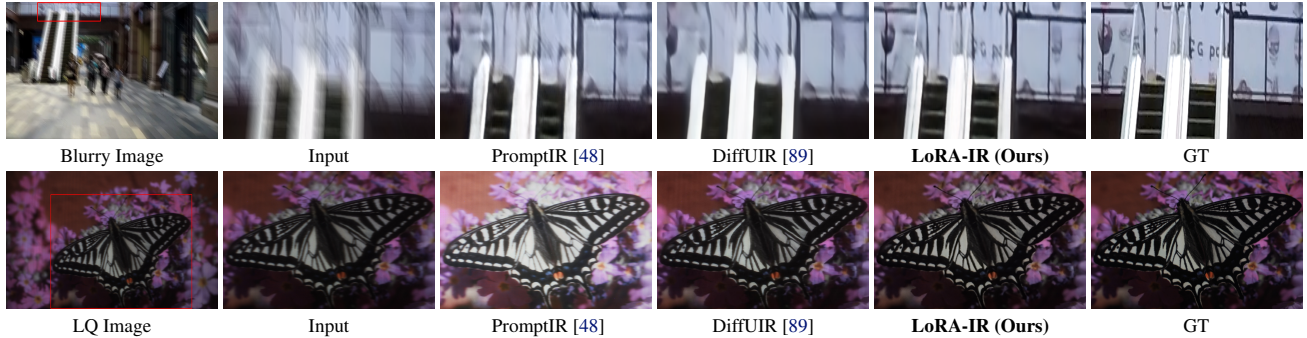


Figure 5. [Setting IV] Visual results on HIDE [55] for *training-seen tasks generalization evaluation* (top row) and TOLED [92] for *training-unseen tasks generalization evaluation* (bottom row). Zoom in for a better view.

Table 4. [Setting IV] Comparison with state-of-the-art task-specific and all-in-one methods for *5-task image restoration*.

Method	Deraining (5sets)		Enhancement		Desnowing (2sets)		Dehazing		Deblurring	
	PSNR $\uparrow$	SSIM $\uparrow$	PSNR $\uparrow$	SSIM $\uparrow$	PSNR $\uparrow$	SSIM $\uparrow$	PSNR $\uparrow$	SSIM $\uparrow$	PSNR $\uparrow$	SSIM $\uparrow$
<b>Task-Specific</b>										
SwinIR [27]	-	-	17.81	0.723	-	-	21.50	0.891	24.52	0.773
MIRNetV2 [79]	-	-	24.74	0.851	-	-	24.03	0.927	26.30	0.799
IR-SDE [35]	-	-	20.45	0.787	-	-	-	-	<b>30.70</b>	<u>0.901</u>
WeatherDiff [46]	-	-	-	-	<u>33.51</u>	<u>0.939</u>	-	-	-	-
RDDM [30]	30.74	0.903	23.22	0.899	<u>32.55</u>	<u>0.927</u>	30.78	0.953	29.53	0.876
<b>All-in-One</b>										
Restormer [78]	27.10	0.843	17.63	0.542	28.61	0.876	22.79	0.706	26.36	0.814
AirNet [22]	24.87	0.773	14.83	0.767	27.63	0.860	25.47	0.923	26.92	0.811
Painter [64]	29.49	0.868	22.40	0.872	-	-	-	-	-	-
IDR [81]	-	-	21.34	0.826	-	-	25.24	0.943	27.87	0.846
ProRes [37]	30.67	0.891	22.73	0.877	-	-	-	-	27.53	0.851
PromptIR [48]	29.56	0.888	22.89	0.847	31.98	0.924	32.02	0.952	27.21	0.817
DACLIP-UIR [36]	28.96	0.853	24.17	0.882	30.80	0.888	31.39	<u>0.983</u>	25.39	0.805
DiffUIR-L [89]	<u>31.03</u>	<u>0.904</u>	<u>25.12</u>	<u>0.907</u>	32.65	0.927	<u>32.94</u>	0.956	29.17	0.864
LoRA-IR (Ours)	<b>32.35</b>	<b>0.924</b>	<b>26.42</b>	<b>0.926</b>	<b>34.16</b>	<b>0.941</b>	<b>35.74</b>	<b>0.986</b>	<u>30.09</u>	<b>0.914</b>

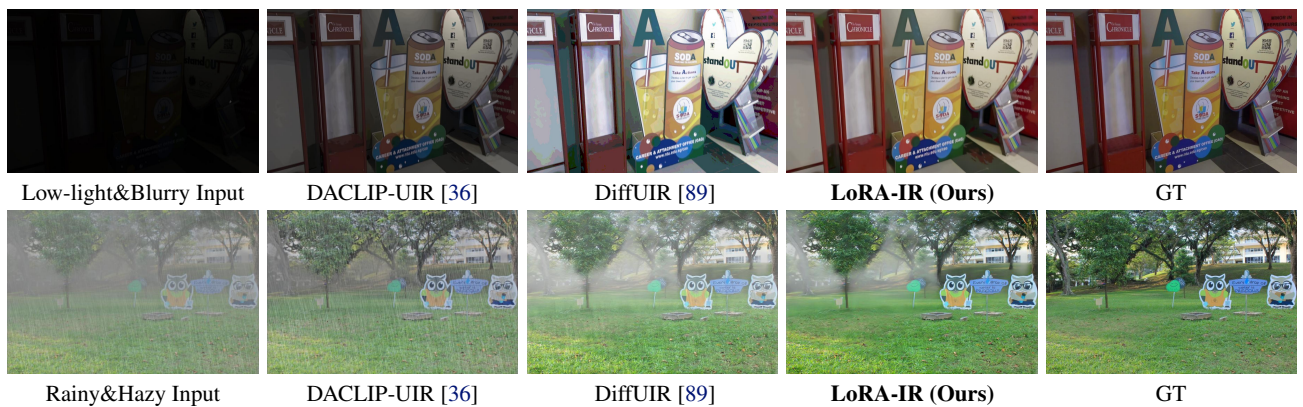


Figure 6. Visual comparisons on challenging *mixed-degradation benchmarks*. Please zoom in for a better view.

comparable or even better performance on no-reference metrics compared to two SOTA diffusion-based methods, DACLIP-UIR [36] and DiffUIR [89]. Notably, our method shows approximately a 100-point improvement in LOE per-

formance over DiffUIR in enhancement. Fig. 5 also shows that our method achieves more pleasing visual results.

(2) *Generalization on Training-unseen Tasks:* We directly test all-in-one models on the training-unseen under-

Table 5. **[Setting IV]** Comparison on real-world benchmarks for *training-seen tasks generalization evaluation*. Best and second best performance of all-in-one approaches are marked in **bold** and underlined, respectively.

Method	Deraining		Enhancement		Desnowing		Deblurring	
	NIQE↓	LOE↓	NIQE↓	LOE↓	NIQE↓	IL-NIQE↓	PSNR↑	SSIM↑
Task-Specific								
WeatherDiff [46]	-	-	-	-	2.96	21.976	-	-
CLIP-LIT [28]	-	-	3.70	232.48	-	-	-	-
RDDM [30]	3.34	41.80	3.57	202.18	2.76	22.261	<u>30.74</u>	<u>0.894</u>
Restormer [78]	3.50	30.32	3.80	351.61	-	-	32.12	0.926
All-in-One								
AirNet [22]	3.55	145.3	3.45	598.13	2.75	<u>21.638</u>	16.78	0.628
PromptIR [48]	3.52	28.53	3.31	255.13	2.79	23.000	22.48	0.770
DACLIP-UIR [36]	3.52	<u>42.03</u>	3.56	218.27	2.72	<b>21.498</b>	17.51	0.667
DiffUIR [89]	<b>3.38</b>	<b>24.82</b>	<b>3.14</b>	<u>193.40</u>	2.74	22.426	30.63	0.890
LoRA-IR (Ours)	<u>3.47</u>	67.53	<u>3.28</u>	<b>93.32</b>	<b>2.70</b>	22.010	<b>30.80</b>	<b>0.907</b>

Table 6. **[Setting IV]** Comparison on TOLED and POLED datasets [92] for *training-unseen tasks generalization evaluation* (under-display camera image restoration).

Method	TOLED [92]			POLED [92]		
	PSNR↑	SSIM↑	LPIPS↓	PSNR↑	SSIM↑	LPIPS↓
NAFNet [4]	26.89	0.774	0.346	10.83	0.416	0.794
HINet [3]	13.84	0.559	0.448	11.52	0.436	0.831
MPRNet [77]	24.69	0.707	0.347	8.34	0.365	0.798
DGUNet [43]	19.67	0.627	0.384	8.88	0.391	0.810
MIRNetV2 [79]	21.86	0.620	0.408	10.27	0.425	0.722
SwinIR [27]	17.72	0.661	0.419	6.89	0.301	0.852
RDDM [30]	23.48	0.639	0.383	15.58	0.398	0.544
Restormer [78]	20.98	0.632	0.360	9.04	0.399	0.742
DL [11]	21.23	0.656	0.434	13.92	0.449	0.756
Transweather [60]	25.02	0.718	0.356	10.46	0.422	0.760
TAPE [31]	17.61	0.583	0.520	7.90	0.219	0.799
AirNet [22]	14.58	0.609	0.445	7.53	0.350	0.820
IDR [81]	27.91	0.795	0.312	<u>16.71</u>	0.497	0.716
PromptIR [48]	16.70	0.688	0.422	13.16	<u>0.583</u>	0.619
DACLIP-UIR [36]	15.74	0.606	0.472	14.91	0.475	0.739
DiffUIR-L [89]	<b>29.55</b>	<b>0.887</b>	<u>0.281</u>	15.62	0.424	<b>0.505</b>
LoRA-IR (Ours)	<u>28.68</u>	<u>0.876</u>	<b>0.279</b>	<b>17.02</b>	<b>0.700</b>	<u>0.600</u>

display camera image restoration task. Tab. 6 shows that, compared to general IR and all-in-one methods, our method achieves either the best or second-best performance across all metrics. Fig. 5 shows that our method produces the clearest result when handling unknown degradations.

**Setting V.** Tab. 7 shows that, compared to DA-CLIP [36], our DG-Router requires significantly fewer (approximately 64×) training parameters and a shorter (about 4×) training time, while achieving more accurate degradation predictions. As shown in Tab. 8, our LoRA-IR outperforms all compared general IR and all-in-one models in both distortion and perceptual metrics, showcasing the superiority of LoRA-IR. The detailed results for each task are provided in the Appendix due to the page limit.

**Mixed-degradation Removal.** Considering that images in real-world scenarios may not contain only a single type of degradation, we further evaluated different all-in-one methods on mixed-degradation benchmarks. Our experiments include three mixed-degradation benchmarks:

Table 7. **[Setting V]** Comparison with DA-CLIP [36] on degradation prediction. Training time is evaluated using A100 GPU hours.

Method	Trainable Params	Training Time	Blur	Haze	JPEG	LL	Noise	RD	Rain	Shadow	Snow	Inpaint
DA-CLIP	94.94M	12	91.6	100	100	100	100	100	100	100	100	100
DG-Router	<b>1.48M</b>	<b>2.67</b>	100	100	100	100	100	100	100	100	100	100

Table 8. **[Setting V]** Quantitative comparisons for *10-task image restoration*. Our LoRA-IR outperforms SOTA methods in both distortion and perceptual metrics.

Method	Distortion		Perceptual	
	PSNR↑	SSIM↑	LPIPS↓	FID↓
NAFNet [4]	26.34	0.847	0.159	55.68
Restormer [78]	26.43	0.850	0.157	54.03
IR-SDE [35]	23.64	0.754	0.167	49.18
AirNet [22]	25.62	0.844	0.182	64.86
PromptIR [48]	<u>27.14</u>	<u>0.859</u>	0.147	48.26
DACLIP-UIR [36]	27.01	<u>0.794</u>	<u>0.127</u>	<u>34.89</u>
LoRA-IR (Ours)	<b>28.64</b>	<b>0.878</b>	<b>0.118</b>	<b>34.26</b>

Table 9. Quantitative comparison with SOTA all-in-one methods on *mixed-degradation benchmarks*. Note that none of the models are trained on mixed-degradation data.

Method	Rain & Haze [23]			Low-light & Blur [91]			Blur & JPEG [45]		
	PSNR↑	SSIM↑	LPIPS↓	PSNR↑	SSIM↑	LPIPS↓	PSNR↑	SSIM↑	LPIPS↓
AirNet [22]	14.02	0.627	0.477	13.84	0.611	0.344	22.79	0.692	0.389
PromptIR [48]	14.75	0.634	0.454	17.61	0.681	0.317	24.98	0.710	0.403
DACLIP-UIR [36]	15.19	0.637	0.481	15.03	0.625	0.330	24.26	0.704	<u>0.358</u>
DiffUIR [89]	<u>14.87</u>	<u>0.631</u>	0.459	15.97	0.657	0.339	24.86	0.714	<b>0.332</b>
LoRA-IR (Ours)	<b>15.41</b>	<b>0.642</b>	<b>0.445</b>	<b>20.59</b>	<b>0.719</b>	<b>0.305</b>	<b>25.05</b>	<b>0.716</b>	0.359

Table 10. Ablations of LoRA-IR on the AllWeather [60] and mixed-degradation benchmarks (Mixed<sub>1</sub>: low-light&blur [91], Mixed<sub>2</sub>: blur&jpeg [45]).

	Snow [34]		Rain [23]		Raindrop [49]		Mixed <sub>1</sub> [91]		Mixed <sub>2</sub> [45]	
	PSNR	SSIM	PSNR	SSIM	PSNR	SSIM	PSNR	SSIM	PSNR	SSIM
DG-Router	32.28	0.930	32.62	0.945	33.39	0.949	20.59	0.719	25.05	0.716
w/o high reso.	32.19	0.929	32.31	0.942			19.51	0.711	24.94	0.714
DAM	32.28	0.930	32.62	0.945	33.39	0.949	20.59	0.719	25.05	0.716
w/o DAM	32.07	0.927	32.28	0.941	33.12	0.945	18.91	0.704	24.89	0.711
AdaLN [47] Modulator	32.13	0.926	32.33	0.938	33.22	0.942	18.44	0.700	24.77	0.705
Mixture of LoRA Expert	32.28	0.930	32.62	0.945	33.39	0.949	20.59	0.719	25.05	0.716
w/o LoRA Expert	32.01	0.925	32.19	0.938	33.03	0.944	16.79	0.675	24.55	0.709

rain&haze [23], low-light&blur [91], and blur&JPEG [45]. Tab. 9 shows that our method has a significant advantage in handling challenging mixed-degradation scenarios. We provide visual results in Fig. 6, showcasing the effectiveness of our method in handling mixed degradations.

### 4.3. Ablation Study

We perform ablation studies to examine the role of each component in our proposed LoRA-IR. To comprehensively validate our method, we conduct experiments on the AllWeather [60] and mixed-degradation [45, 91] benchmarks. In Tab. 10, we start with LoRA-IR and systematically remove or replace modules, including the high-resolution techniques in DG-Router, the DAM module (we also at-

tempt to use AdaLN [47] for feature modulation), and the mixture of LoRA expert design. We find that LoRA-IR consistently outperforms its ablated versions across all benchmarks, highlighting the critical importance of these components. Notably, our mixture of LoRA expert design significantly improves the model’s performance on mixed-degradation benchmarks, enhancing the model’s generalizability in real-world scenarios. More detailed ablations, model efficiency comparison and analysis are provided in the Appendix.

## 5. Conclusion

This paper introduces LoRA-IR, a flexible framework that dynamically leverages compact low-rank experts to facilitate efficient all-in-one image restoration. We propose a CLIP-based degradation-guided router (DG-Router) to extract robust degradation representations, requiring minimal training parameters and time. With the valuable guidance of the DG-Router, LoRA-IR dynamically integrates different low-rank experts, enhancing architectural flexibility while preserving computational efficiency. Across 14 image restoration tasks and 29 benchmarks, LoRA-IR demonstrates its state-of-the-art performance and strong generalizability.

## References

- [1] Josh Achiam, Steven Adler, Sandhini Agarwal, Lama Ahmad, Ilge Akkaya, Florencia Leoni Aleman, Diogo Almeida, Janko Altmenschmidt, Sam Altman, Shyamal Anadkat, et al. Gpt-4 technical report. *arXiv preprint arXiv:2303.08774*, 2023. 3
- [2] Yuang Ai, Huaibo Huang, Xiaoqiang Zhou, Jiexiang Wang, and Ran He. Multimodal prompt perceiver: Empower adaptiveness generalizability and fidelity for all-in-one image restoration. In *CVPR*, pages 25432–25444, 2024. 1, 3, 5, 6
- [3] Liangyu Chen, Xin Lu, Jie Zhang, Xiaojie Chu, and Chengpeng Chen. Hinet: Half instance normalization network for image restoration. In *CVPR*, pages 182–192, 2021. 8
- [4] Liangyu Chen, Xiaojie Chu, Xiangyu Zhang, and Jian Sun. Simple baselines for image restoration. In *ECCV*, pages 17–33, 2022. 3, 5, 6, 8
- [5] Wei-Ting Chen, Hao-Yu Fang, Jian-Jiun Ding, Cheng-Che Tsai, and Sy-Yen Kuo. Jstasr: Joint size and transparency-aware snow removal algorithm based on modified partial convolution and veiling effect removal. In *ECCV*, pages 754–770, 2020. 6
- [6] Wei-Ting Chen, Zhi-Kai Huang, Cheng-Che Tsai, Hao-Hsiang Yang, Jian-Jiun Ding, and Sy-Yen Kuo. Learning multiple adverse weather removal via two-stage knowledge learning and multi-contrastive regularization: Toward a unified model. In *CVPR*, pages 17653–17662, 2022. 6
- [7] Xiang Chen, Hao Li, Mingqiang Li, and Jinshan Pan. Learning a sparse transformer network for effective image deraining. In *CVPR*, pages 5896–5905, 2023. 1
- [8] Mehdi Cherti, Romain Beaumont, Ross Wightman, Mitchell Wortsman, Gabriel Ilharco, Cade Gordon, Christoph Schuhmann, Ludwig Schmidt, and Jenia Jitsev. Reproducible scaling laws for contrastive language-image learning. In *CVPR*, pages 2818–2829, 2023. 3
- [9] Yuning Cui, Wenqi Ren, Xiaochun Cao, and Alois Knoll. Focal network for image restoration. In *ICCV*, pages 13001–13011, 2023. 3
- [10] Yu Dong, Yihao Liu, He Zhang, Shifeng Chen, and Yu Qiao. Fd-gan: Generative adversarial networks with fusion-discriminator for single image dehazing. In *AAAI*, pages 10729–10736, 2020. 6
- [11] Qingnan Fan, Dongdong Chen, Lu Yuan, Gang Hua, Nenghai Yu, and Baoquan Chen. A general decoupled learning framework for parameterized image operators. *TPAMI*, 43(1):33–47, 2019. 6, 8
- [12] Hongyun Gao, Xin Tao, Xiaoyong Shen, and Jiaya Jia. Dynamic scene deblurring with parameter selective sharing and nested skip connections. In *CVPR*, pages 3848–3856, 2019. 6
- [13] Martin Heusel, Hubert Ramsauer, Thomas Unterthiner, Bernhard Nessler, and Sepp Hochreiter. Gans trained by a two time-scale update rule converge to a local nash equilibrium. In *NeurIPS*, pages 6626–6637, 2017. 5
- [14] Edward J Hu, Yelong Shen, Phillip Wallis, Zeyuan Allen-Zhu, Yuanzhi Li, Shean Wang, Lu Wang, and Weizhu Chen. LoRA: Low-rank adaptation of large language models. In *ICLR*, 2022. 2, 3
- [15] Huaibo Huang, Aijing Yu, and Ran He. Memory oriented transfer learning for semi-supervised image deraining. In *CVPR*, pages 7732–7741, 2021. 1
- [16] Phillip Isola, Jun-Yan Zhu, Tinghui Zhou, and Alexei A Efros. Image-to-image translation with conditional adversarial networks. In *CVPR*, 2017. 6
- [17] Kui Jiang, Zhongyuan Wang, Peng Yi, Chen Chen, Zheng Wang, Xiao Wang, Junjun Jiang, and Chia-Wen Lin. Rain-free and residue hand-in-hand: A progressive coupled network for real-time image deraining. *TIP*, 2021. 6
- [18] Alexander Kirillov, Eric Mintun, Nikhila Ravi, Hanzi Mao, Chloe Rolland, Laura Gustafson, Tete Xiao, Spencer Whitehead, Alexander C Berg, Wan-Yen Lo, et al. Segment anything. In *ICCV*, pages 4015–4026, 2023. 3
- [19] Chulwoo Lee, Chul Lee, and Chang-Su Kim. Contrast enhancement based on layered difference representation of 2d histograms. *TIP*, 22(12):5372–5384, 2013. 5
- [20] Brian Lester, Rami Al-Rfou, and Noah Constant. The power of scale for parameter-efficient prompt tuning. In *EMNLP*, pages 3045–3059, 2021. 3
- [21] Boyi Li, Wenqi Ren, Dengpan Fu, Dacheng Tao, Dan Feng, Wenjun Zeng, and Zhangyang Wang. Benchmarking single-image dehazing and beyond. *TIP*, 28(1):492–505, 2018. 5
- [22] Boyun Li, Xiao Liu, Peng Hu, Zhongqin Wu, Jiancheng Lv, and Xi Peng. All-in-one image restoration for unknown corruption. In *CVPR*, pages 17452–17462, 2022. 3, 5, 6, 7, 8
- [23] Ruoteng Li, Loong-Fah Cheong, and Robby T Tan. Heavy rain image restoration: Integrating physics model and con-

- ditional adversarial learning. In *CVPR*, pages 1633–1642, 2019. 6, 8
- [24] Ruoteng Li, Robby T Tan, and Loong-Fah Cheong. All in one bad weather removal using architectural search. In *CVPR*, pages 3175–3185, 2020. 1, 6
- [25] Xia Li, Jianlong Wu, Zhouchen Lin, Hong Liu, and Hongbin Zha. Recurrent squeeze-and-excitation context aggregation net for single image deraining. In *ECCV*, 2018. 6
- [26] Yawei Li, Yuchen Fan, Xiaoyu Xiang, Denis Demandolx, Rakesh Ranjan, Radu Timofte, and Luc Van Gool. Efficient and explicit modelling of image hierarchies for image restoration. In *CVPR*, pages 18278–18289, 2023. 3, 6
- [27] Jingyun Liang, Jiezhong Cao, Guolei Sun, Kai Zhang, Luc Van Gool, and Radu Timofte. Swinir: Image restoration using swin transformer. In *ICCVW*, pages 1833–1844, 2021. 3, 7, 8
- [28] Zhixin Liang, Chongyi Li, Shangchen Zhou, Ruicheng Feng, and Chen Change Loy. Iterative prompt learning for unsupervised backlit image enhancement. In *ICCV*, pages 8094–8103, 2023. 8
- [29] Haotian Liu, Chunyuan Li, Qingyang Wu, and Yong Jae Lee. Visual instruction tuning. In *NeurIPS*, 2024. 2, 3
- [30] Jiawei Liu, Qiang Wang, Huijie Fan, Yinong Wang, Yandong Tang, and Liangqiong Qu. Residual denoising diffusion models. In *CVPR*, pages 2773–2783, 2024. 7, 8
- [31] Lin Liu, Lingxi Xie, Xiaopeng Zhang, Shanxin Yuan, Xiangyu Chen, Wengang Zhou, Houqiang Li, and Qi Tian. Tape: Task-agnostic prior embedding for image restoration. In *ECCV*, pages 447–464, 2022. 8
- [32] Xing Liu, Masanori Suganuma, Zhun Sun, and Takayuki Okatani. Dual residual networks leveraging the potential of paired operations for image restoration. In *CVPR*, 2019. 6
- [33] Yihao Liu, Xiangyu Chen, Xianzheng Ma, Xintao Wang, Jiantao Zhou, Yu Qiao, and Chao Dong. Unifying image processing as visual prompting question answering. In *ICML*, 2024. 1
- [34] Yun-Fu Liu, Da-Wei Jaw, Shih-Chia Huang, and Jenq-Neng Hwang. Desnownet: Context-aware deep network for snow removal. *TIP*, 27(6):3064–3073, 2018. 5, 6, 8
- [35] Ziwei Luo, Fredrik K Gustafsson, Zheng Zhao, Jens Sjölund, and Thomas B Schön. Image restoration with mean-reverting stochastic differential equations. In *ICML*, pages 23045–23066, 2023. 7, 8
- [36] Ziwei Luo, Fredrik K Gustafsson, Zheng Zhao, Jens Sjölund, and Thomas B Schön. Controlling vision-language models for universal image restoration. In *ICLR*, 2024. 1, 3, 5, 7, 8
- [37] Jiaqi Ma, Tianheng Cheng, Guoli Wang, Qian Zhang, Xinggang Wang, and Lefei Zhang. Prores: Exploring degradation-aware visual prompt for universal image restoration. *arXiv preprint arXiv:2306.13653*, 2023. 7
- [38] Kede Ma, Kai Zeng, and Zhou Wang. Perceptual quality assessment for multi-exposure image fusion. *TIP*, 24(11):3345–3356, 2015. 5
- [39] Kede Ma, Zhengfang Duanmu, Qingbo Wu, Zhou Wang, Hongwei Yong, Hongliang Li, and Lei Zhang. Waterloo exploration database: New challenges for image quality assessment models. *TIP*, 26(2):1004–1016, 2016. 5
- [40] Jiayuan Mao, Tete Xiao, Yuning Jiang, and Zhimin Cao. What can help pedestrian detection? In *CVPR*, pages 3127–3136, 2017. 1
- [41] David Martin, Charless Fowlkes, Doron Tal, and Jitendra Malik. A database of human segmented natural images and its application to evaluating segmentation algorithms and measuring ecological statistics. In *ICCV*, pages 416–423, 2001. 5
- [42] Anish Mittal, Rajiv Soundararajan, and Alan C Bovik. Making a “completely blind” image quality analyzer. *IEEE Signal processing letters*, 20(3):209–212, 2012. 5
- [43] Chong Mou, Qian Wang, and Jian Zhang. Deep generalized unfolding networks for image restoration. In *CVPR*, pages 17399–17410, 2022. 8
- [44] Seungjun Nah, Tae Hyun Kim, and Kyoung Mu Lee. Deep multi-scale convolutional neural network for dynamic scene deblurring. In *CVPR*, pages 3883–3891, 2017. 3, 5
- [45] Seungjun Nah, Sungyong Baik, Seokil Hong, Gyeongsik Moon, Sanghyun Son, Radu Timofte, and Kyoung Mu Lee. Reds. In *CVPRW*, 2019. 8
- [46] Ozan Özdenizci and Robert Legenstein. Restoring vision in adverse weather conditions with patch-based denoising diffusion models. *TPAMI*, 45(8):10346–10357, 2023. 6, 7, 8
- [47] Ethan Perez, Florian Strub, Harm De Vries, Vincent Dumoulin, and Aaron Courville. Film: Visual reasoning with a general conditioning layer. In *AAAI*, 2018. 8, 9
- [48] Vaishnav Potlapalli, Syed Waqas Zamir, Salman H Khan, and Fahad Shahbaz Khan. Promptir: Prompting for all-in-one image restoration. In *NeurIPS*, pages 71275–71293, 2023. 1, 3, 6, 7, 8
- [49] Rui Qian, Robby T Tan, Wenhan Yang, Jiajun Su, and Jiaying Liu. Attentive generative adversarial network for raindrop removal from a single image. In *CVPR*, pages 2482–2491, 2018. 6, 8
- [50] Yuhui Quan, Shijie Deng, Yixin Chen, and Hui Ji. Deep learning for seeing through window with raindrops. In *ICCV*, pages 2463–2471, 2019. 6
- [51] Alec Radford, Jong Wook Kim, Chris Hallacy, Aditya Ramesh, Gabriel Goh, Sandhini Agarwal, Girish Sastry, Amanda Askell, Pamela Mishkin, Jack Clark, et al. Learning transferable visual models from natural language supervision. In *ICML*, pages 8748–8763, 2021. 2, 3
- [52] Jaesung Rim, Haeyun Lee, Jucheol Won, and Sunghyun Cho. Real-world blur dataset for learning and benchmarking deblurring algorithms. In *ECCV*, pages 184–201, 2020. 5
- [53] Noam Shazeer, Azalia Mirhoseini, Krzysztof Maziarz, Andy Davis, Quoc Le, Geoffrey Hinton, and Jeff Dean. Outrageously large neural networks: The sparsely-gated mixture-of-experts layer. *arXiv preprint arXiv:1701.06538*, 2017. 2
- [54] HR Sheikh. Live image quality assessment database release 2. <http://live.ece.utexas.edu/research/quality>, 2005. 3
- [55] Ziyi Shen, Wenguan Wang, Xiankai Lu, Jianbing Shen, Haibin Ling, Tingfa Xu, and Ling Shao. Human-aware motion deblurring. In *ICCV*, pages 5572–5581, 2019. 5, 7
- [56] Shangquan Sun, Wenqi Ren, Xinwei Gao, Rui Wang, and Xiaochun Cao. Restoring images in adverse weather conditions via histogram transformer. In *ECCV*, 2024. 5, 6

- [57] Chunwei Tian, Yong Xu, and Wangmeng Zuo. Image denoising using deep cnn with batch renormalization. *Neural Networks*, 121:461–473, 2020. 6
- [58] Fu-Jen Tsai, Yan-Tsung Peng, Yen-Yu Lin, Chung-Chi Tsai, and Chia-Wen Lin. Stripformer: Strip transformer for fast image deblurring. In *ECCV*, pages 146–162, 2022. 1
- [59] Zhengzhong Tu, Hossein Talebi, Han Zhang, Feng Yang, Peyman Milanfar, Alan Bovik, and Yinxiao Li. Maxim: Multi-axis mlp for image processing. In *CVPR*, pages 5769–5780, 2022. 6
- [60] Jeya Maria Jose Valanarasu, Rajeev Yasarla, and Vishal M Patel. Transweather: Transformer-based restoration of images degraded by adverse weather conditions. In *CVPR*, pages 2353–2363, 2022. 3, 5, 6, 8
- [61] Shuhang Wang, Jin Zheng, Hai-Miao Hu, and Bo Li. Naturalness preserved enhancement algorithm for non-uniform illumination images. *TIP*, 22(9):3538–3548, 2013. 5
- [62] Shuhang Wang, Jin Zheng, Hai-Miao Hu, and Bo Li. Naturalness preserved enhancement algorithm for non-uniform illumination images. *TIP*, 22(9):3538–3548, 2013. 5
- [63] Tianyu Wang, Xin Yang, Ke Xu, Shaozhe Chen, Qiang Zhang, and Rynson WH Lau. Spatial attentive single-image deraining with a high quality real rain dataset. In *CVPR*, 2019. 6
- [64] Xinlong Wang, Wen Wang, Yue Cao, Chunhua Shen, and Tiejun Huang. Images speak in images: A generalist painter for in-context visual learning. In *CVPR*, pages 6830–6839, 2023. 7
- [65] Zhendong Wang, Xiaodong Cun, Jianmin Bao, Wengang Zhou, Jianzhuang Liu, and Houqiang Li. Uformer: A general u-shaped transformer for image restoration. In *CVPR*, pages 17683–17693, 2022. 3, 6
- [66] Zhengbo Wang, Jian Liang, Ran He, Nan Xu, Zilei Wang, and Tieniu Tan. Improving zero-shot generalization for clip with synthesized prompts. In *ICCV*, pages 3032–3042, 2023. 3
- [67] Zhengbo Wang, Jian Liang, Lijun Sheng, Ran He, Zilei Wang, and Tieniu Tan. A hard-to-beat baseline for training-free clip-based adaptation. In *ICLR*, 2024. 3
- [68] Chen Wei, Wenjing Wang, Wenhan Yang, and Jiaying Liu. Deep retinex decomposition for low-light enhancement. *arXiv preprint arXiv:1808.04560*, 2018. 5
- [69] Rongyuan Wu, Tao Yang, Lingchen Sun, Zhengqiang Zhang, Shuai Li, and Lei Zhang. Seesr: Towards semantics-aware real-world image super-resolution. In *CVPR*, 2024. 6
- [70] Yuhui Wu, Chen Pan, Guoqing Wang, Yang Yang, Jiwei Wei, Chongyi Li, and Heng Tao Shen. Learning semantic-aware knowledge guidance for low-light image enhancement. In *CVPR*, pages 1662–1671, 2023. 1
- [71] Bin Xia, Yulun Zhang, Shiyin Wang, Yitong Wang, Xinglong Wu, Yapeng Tian, Wenming Yang, and Luc Van Gool. Diffir: Efficient diffusion model for image restoration. In *ICCV*, pages 13095–13105, 2023. 3
- [72] Jie Xiao, Xueyang Fu, Aiping Liu, Feng Wu, and Zheng-Jun Zha. Image de-raining transformer. *TPAMI*, 45(11):12978–12995, 2023. 6
- [73] Hao Yang, Liyuan Pan, Yan Yang, and Wei Liang. Language-driven all-in-one adverse weather removal. In *CVPR*, pages 24902–24912, 2024. 5, 6
- [74] Wenhan Yang, Robby T Tan, Jiashi Feng, Jiaying Liu, Zongming Guo, and Shuicheng Yan. Deep joint rain detection and removal from a single image. In *CVPR*, pages 1357–1366, 2017. 5
- [75] Tian Ye, Sixiang Chen, Jinbin Bai, Jun Shi, Chenghao Xue, Jingxia Jiang, Junjie Yin, Er kang Chen, and Yun Liu. Adverse weather removal with codebook priors. In *ICCV*, 2023. 6
- [76] Fanghua Yu, Jinjin Gu, Zheyuan Li, Jinfan Hu, Xiangtao Kong, Xintao Wang, Jingwen He, Yu Qiao, and Chao Dong. Scaling up to excellence: Practicing model scaling for photo-realistic image restoration in the wild. In *CVPR*, 2024. 6
- [77] Syed Waqas Zamir, Aditya Arora, Salman Khan, Munawar Hayat, Fahad Shahbaz Khan, Ming-Hsuan Yang, and Ling Shao. Multi-stage progressive image restoration. In *CVPR*, pages 14821–14831, 2021. 3, 6, 8
- [78] Syed Waqas Zamir, Aditya Arora, Salman Khan, Munawar Hayat, Fahad Shahbaz Khan, and Ming-Hsuan Yang. Restormer: Efficient transformer for high-resolution image restoration. In *CVPR*, pages 5728–5739, 2022. 3, 5, 6, 7, 8
- [79] Syed Waqas Zamir, Aditya Arora, Salman Khan, Munawar Hayat, Fahad Shahbaz Khan, Ming-Hsuan Yang, and Ling Shao. Learning enriched features for fast image restoration and enhancement. *TPAMI*, 45(2):1934–1948, 2022. 7, 8
- [80] Howard Zhang, Yunhao Ba, Ethan Yang, Varan Mehra, Blake Gella, Akira Suzuki, Arnold Pfahnl, Chethan Chindera Chandrappa, Alex Wong, and Achuta Kadambi. Weatherstream: Light transport automation of single image deweathering. In *CVPR*, pages 13499–13509, 2023. 2, 5, 6
- [81] Jinghao Zhang, Jie Huang, Mingde Yao, Zizheng Yang, Hu Yu, Man Zhou, and Feng Zhao. Ingredient-oriented multi-degradation learning for image restoration. In *CVPR*, pages 5825–5835, 2023. 3, 7, 8
- [82] Jiale Zhang, Yulun Zhang, Jinjin Gu, Yongbing Zhang, Linghe Kong, and Xin Yuan. Accurate image restoration with attention retractable transformer. In *ICLR*, 2023. 3
- [83] Kai Zhang, Wangmeng Zuo, Yunjin Chen, Deyu Meng, and Lei Zhang. Beyond a gaussian denoiser: Residual learning of deep cnn for image denoising. *TIP*, 26(7):3142–3155, 2017. 1
- [84] Kaihao Zhang, Rongqing Li, Yanjiang Yu, Wenhan Luo, and Changsheng Li. Deep dense multi-scale network for snow removal using semantic and depth priors. *TIP*, 30:7419–7431, 2021. 6
- [85] Lin Zhang, Lei Zhang, and Alan C Bovik. A feature-enriched completely blind image quality evaluator. *TIP*, 24(8):2579–2591, 2015. 5
- [86] Lvmin Zhang, Anyi Rao, and Maneesh Agrawala. Adding conditional control to text-to-image diffusion models. In *ICCV*, pages 3836–3847, 2023. 3
- [87] Richard Zhang, Phillip Isola, Alexei A Efros, Eli Shechtman, and Oliver Wang. The unreasonable effectiveness of deep features as a perceptual metric. In *CVPR*, pages 586–595, 2018. 5

- [88] Yulun Zhang, Kunpeng Li, Kai Li, Lichen Wang, Bineng Zhong, and Yun Fu. Image super-resolution using very deep residual channel attention networks. In *ECCV*, pages 286–301, 2018. 4
- [89] Dian Zheng, Xiao-Ming Wu, Shuzhou Yang, Jian Zhang, Jian-Fang Hu, and Wei-Shi Zheng. Selective hourglass mapping for universal image restoration based on diffusion model. In *CVPR*, pages 25445–25455, 2024. 5, 6, 7, 8
- [90] Kaiyang Zhou, Jingkang Yang, Chen Change Loy, and Ziwei Liu. Learning to prompt for vision-language models. *IJCV*, 130(9):2337–2348, 2022. 2, 3
- [91] Shangchen Zhou, Chongyi Li, and Chen Change Loy. Lednet: Joint low-light enhancement and deblurring in the dark. In *ECCV*, pages 573–589, 2022. 8
- [92] Yuqian Zhou, David Ren, Neil Emerton, Sehoon Lim, and Timothy Large. Image restoration for under-display camera. In *CVPR*, pages 9179–9188, 2021. 7, 8
- [93] Ziqin Zhou, Yinjie Lei, Bowen Zhang, Lingqiao Liu, and Yifan Liu. Zegclip: Towards adapting clip for zero-shot semantic segmentation. In *CVPR*, pages 11175–11185, 2023. 3
- [94] Jun-Yan Zhu, Taesung Park, Phillip Isola, and Alexei A Efros. Unpaired image-to-image translation using cycle-consistent adversarial networks. In *ICCV*, 2017. 6
- [95] Yurui Zhu, Tianyu Wang, Xueyang Fu, Xuanyu Yang, Xin Guo, Jifeng Dai, Yu Qiao, and Xiaowei Hu. Learning weather-general and weather-specific features for image restoration under multiple adverse weather conditions. In *CVPR*, pages 21747–21758, 2023. 2, 3, 6
- [96] Zhe Zhu, Dun Liang, Songhai Zhang, Xiaolei Huang, Baoli Li, and Shimin Hu. Traffic-sign detection and classification in the wild. In *CVPR*, pages 2110–2118, 2016. 1